A genetic system to study *Plasmodium falciparum* protein function

Jakob Birnbaum[1,2], Sven Flemming[1,2], Nick Reichard[1], Alexandra Blancke Soares[1], Paolo Mesén-Ramírez[1], Ernst Jonscher[1], Bärbel Bergmann[1] & Tobias Spielmann[1]

Current systems to study essential genes in the human malaria parasite *Plasmodium falciparum* are often inefficient and time intensive, and they depend on the genetic modification of the target locus, a process hindered by the low frequency of integration of episomal DNA into the genome. Here, we introduce a method, termed selection-linked integration (SLI), to rapidly select for genomic integration. SLI allowed us to functionally analyze targets at the gene and protein levels, thus permitting mislocalization of native proteins, a strategy known as knock sideways, floxing to induce diCre-based excision of genes and knocking in altered gene copies. We demonstrated the power and robustness of this approach by validating it for more than 12 targets, including eight essential ones. We also localized and inducibly inactivated Kelch13, the protein associated with artemisinin resistance. We expect this system to be widely applicable for *P. falciparum* and other organisms with limited genetic tractability.

The most severe form of malaria, caused by the protozoan parasite *P. falciparum*, is a major health problem, and substantial efforts are currently being made to combat this disease[1]. Nonetheless, little is known about many aspects of this parasite's biology. Approximately 50% of the predicted *P. falciparum* gene products have unknown functions[2]. Localization and functional analysis of these proteins are essential to understand the biology of this parasite and to uncover new drug targets, but progress in this respect has been slow[2,3]. It has been estimated that it will take until 2050 to localize all proteins of this parasite[4], and endogenous tagging of all native proteins with GFP, an endeavor that has been immensely useful in other systems[5], is even further away.

Similarly, the rate at which *P. falciparum* genes are being functionally analyzed is low[2]. Although there have been great advances permitting the functional study of a limited number of genes, the targeted inactivation of *P. falciparum* genes is still labor intensive and limited in throughput, and the success is often uncertain[2,3] (**Supplementary Table 1**). These drawbacks are particularly relevant for essential genes, because parasites with genetic changes detrimental to survival are difficult to obtain. A general problem is that homologous recombination is inefficient and passively selected for by drug cycling. As a result, even simple modifications, such as GFP knockins or gene disruptions, are often obtained only after many months, if at all.

Here, we introduce a simple and robust technique that dramatically increases the speed and success rate in obtaining cell lines with genomic integrations in *P. falciparum*. With this system, we (i) localized native proteins by fusing them with GFP, (ii) disrupted genes, (iii) knocked in an allele conferring artemisinin resistance and (iv) performed functional analyses of known and newly identified essential genes at the protein level, by using knock sideways (KS)[6–8] and diCre-based[9–11] inducible gene deletion. This analysis included the *P. falciparum* artemisinin-resistance protein Kelch13 (ref. 12), which has not previously been localized or directly targeted. These methods enable the medium-throughput analysis of *P. falciparum* gene products and should be equally useful for other organisms with limited genetic tractability.

RESULTS

Efficient selection of genomic integration

To overcome the inefficiency of homologous recombination in *P. falciparum*, we developed a method permitting the selection of parasites with genomic integrations, which we termed selection-linked integration. In this approach, a promoterless targeting region on the plasmid to be integrated is linked with an additional selectable marker that is separated by a skip peptide[13,14]. This additional selectable marker can be expressed only after single crossover integration into the target locus, but because of the skip peptide, the marker is not attached to the target itself (**Fig. 1a**). Hence, parasites carrying the integration can be selected by using the additional integration-linked resistance marker (denoted the SLI-resistance marker).

To test the SLI method, we generated GFP knockins (full-length endogenous genes fused to a *gfp* sequence). As an SLI-resistance marker, we chose neomycin phosphotransferase[15], an infrequently used marker in *P. falciparum* research. After transfection and selection of parasites bearing the episomal plasmid, integration via SLI was compared with conventional drug cycling for four genes targeted in this work. With SLI, we obtained cell lines with the correct integration after 5–16 d of neomycin

[1]Bernhard Nocht Institute for Tropical Medicine, Parasitology Section, Hamburg, Germany. [2]These authors contributed equally to this work. Correspondence should be addressed to T.S. (spielmann@bni-hamburg.de).

RECEIVED 23 SEPTEMBER 2016; ACCEPTED 6 FEBRUARY 2017; PUBLISHED ONLINE 13 MARCH 2017; DOI:10.1038/NMETH.4223

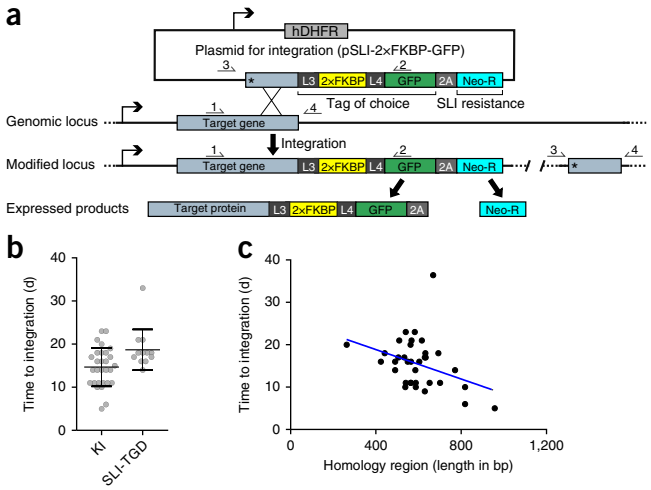

Figure 1 | Selection-linked integration and knock sideways. (**a**) Schematic of SLI strategy. L3 and L4 are linkers[35]; 2A, T2A skip peptide; Neo-R, neomycin-resistance gene; asterisks, stop codons; arrows, promoters. (**b**) Plot of time to integration for all cell lines generated for this study by using SLI, separated in GFP-knockin (KI) and SLI-TGD (see **Fig. 4**). Data are shown as mean ± s.d. (n = 29 integration cell lines for KI and 11 integration cell lines for SLI-TGD). (**c**) Time to integration plotted versus targeting-region length for all integration cell lines in this study in which neomycin was used as a C-terminal SLI-resistance marker.

selection (**Supplementary Fig. 1a**,**b**). In contrast, via drug cycling, two plasmids did not integrate (after 3 months), and two required 59 d to show integration (**Supplementary Fig. 1a**). Immunoblot analysis confirmed quantitative skipping to remove the SLI-resistance marker from the target after integration (**Supplementary Fig. 2a**). Similar results were obtained with two plasmids with a different SLI-resistance marker (blasticidin-S deaminase) (**Supplementary Fig. 1**).

In this study, SLI was used to establish 40 integration cell lines, which were obtained 15.8 (±5.0) d after selection for integration (**Fig. 1b**). The time to integration correlated with the length of the targeting region (**Fig. 1c**) but not the expression levels of the target (**Supplementary Fig. 2b**).

Functional analysis of essential *P. falciparum* proteins with knock sideways

Current gene and protein inactivation methods in *P. falciparum* have limitations (**Supplementary Table 1**). We therefore chose KS, originally called anchor away, as an alternative[6–8,16–18]. KS is based on the ligand-induced dimerization of the proteins FRB* and FKBP. The native target is fused with FKBP, whereas FRB* is separately expressed with the trafficking information for a different cellular compartment (the 'mislocalizer'). After addition of the ligand (rapalog) to dimerize FRB* and FKBP, the target protein is removed from its site of action by the mislocalizer (**Supplementary Fig. 2c**). This method acts rapidly and avoids the problems of targeting essential genes at the genetic level. Because we used a GFP tag together with FKBP (**Fig. 1a**), the native target is also localized.

A proof-of-principle experiment indicated that rapalog-dependent dimerization of FKBP and FRB* was feasible in *P. falciparum* (**Supplementary Fig. 2d**,**e**). To test KS with actual targets, we endogenously tagged two known essential proteins, CDPK5 (ref. 19) and HP1 (ref. 20), with 2×FKBP-GFP, by using SLI (**Supplementary Fig. 1b**). CDPK5-2×FKBP-GFP was expressed in late schizonts, in which it showed a diffuse uniform localization with multiple foci (**Fig. 2a**). HP1-2×FKBP-GFP was located at the nucleus (**Fig. 2b**), as previously described[20]. We used a nuclear mislocalizer for CDPK5 and a plasma-membrane mislocalizer for HP1. Addition of rapalog caused efficient transfer of CDPK5-2×FKBP-GFP into the nucleus, whereas 95.8% (s.d. 3.7%, n = 11 cells) of HP1-2×FKBP-GFP was relocated from the nucleus to the plasma membrane (**Fig. 2a**,**b**). Growth assays after KS confirmed that both proteins are important for parasite proliferation (**Fig. 2a**,**b**). Rapalog treated wild-type parasites expressing the mislocalizers without an FKBP-tagged target showed no difference compared with the control, thus excluding any effect of rapalog or the mislocalizer itself (**Supplementary Fig. 3**). In synchronized parasites, KS of CDPK5 caused an accumulation of segmented schizonts (**Fig. 2a**), in agreement with the previously described egress phenotype[19]. Mislocalization of HP1 caused an accumulation of gametocytes (**Fig. 2b**), thus also confirming previous data[20].

Next, we analyzed targets that had not previously been functionally characterized in *P. falciparum*. We chose two proteins containing domains involved in vesicular trafficking, annotated as ArfGAP (PF3D7_1244600) and Mon1 (PF3D7_1352800). Both proteins were found in foci in the cytoplasm of the parasite (**Supplementary Fig. 4a**,**b**). For both proteins, KS left no detectable foci in the cytoplasm and indicated that Mon1 is important for parasite schizont development, whereas ArfGAP is dispensable for blood-stage growth (**Supplementary Fig. 4**). Overall these data showed that KS is useful for the functional analysis of essential proteins in this parasite.

N-terminal tagging and validation of KS by genetic deletion and complementation

Next, we tested whether KS can also be used in proteins requiring N-terminal tagging. To do so, we chose PfRab5a, which has previously been implicated in hemoglobin uptake in intracellular blood stages[21]. Rab5a cannot be tagged C-terminally, owing to the need for C-terminal prenylation. We replaced the prenylation motif of endogenous Rab5a to inactivate it and added a functional N-terminally GFP-2×FKBP-tagged copy of Rab5a via a skip peptide, thus enabling expression from the endogenous locus. We also added *loxP* sites 5′ and 3′ of the functional copy (**Supplementary Fig. 5a**). The knockin cell line (**Supplementary Fig. 5b**) showed that GFP-2×FKBP-Rab5a was located in several foci in the parasite cytosol (**Fig. 3a**), some of which were proximal to the nucleus (**Supplementary Fig. 5c**).

We then generated three different GFP-2×FKBP-Rab5a parasite lines to perform KS with a nuclear mislocalizer (cell line 1), KS in the presence of a complementary copy of Rab5a (cell line 2) or excision of the functional gene with inducible Cre recombinase[9–11] (cell line 3). After addition of rapalog to cell line 1, GFP-2×FKBP-Rab5a was efficiently mislocalized into the nucleus, and no detectable protein remained in the cytoplasm (**Fig. 3a**). KS abolished parasite growth, owing to a growth arrest in late schizonts (**Fig. 3a**). In contrast, the second cell line, which expressed a complementary copy of Rab5a in addition to GFP-2×FKBP-Rab5a, grew normally after rapalog addition (**Fig. 3b**). In the third cell line, rapalog addition to dimerize split Cre led to excision of the functional copy of *rab5a* and to a phenotype comparable

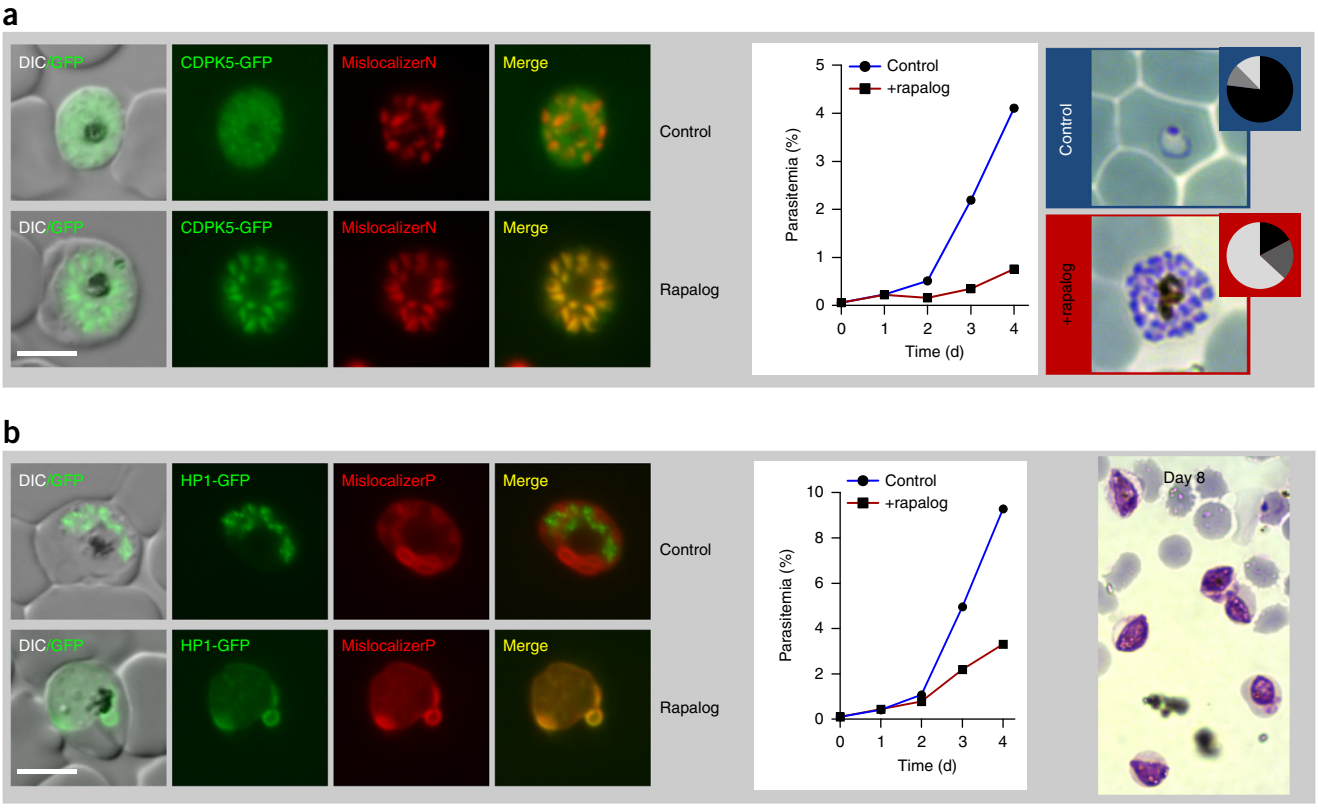

Figure 2 | Localization and KS with protein targets. (**a**,**b**) Knockin cell lines of CDPK5-2×FKBP-GFP with an mCherry-tagged nuclear mislocalizer (MislocalizerN) (**a**) and HP1-2×FKBP-GFP with a plasma-membrane mislocalizer (MislocalizerP) (**b**). Representative fluorescence microscopy images of rapalog-treated and control cells (after 16 h) are shown next to flow cytometry (FC) growth curves (one representative of the 3 independent experiments in **Supplementary Fig. 3** is shown). In **a**, right images show Giemsa-stained blood smears after the first development cycle of synchronized parasites. Pie charts for CDPK5 show quantification of stages (rings, black; trophozoites, dark gray; schizonts, light gray; n = 226 and 255 cells for control and +rapalog, respectively). One representative of 3 independent experiments is shown. Giemsa-stained smears in **b** show gametocytes 8 d after initiation of KS (one representative of two independent experiments is shown). DIC, differential interference contrast; merge, merged red and green signal; asterisk, food-vacuole autofluorescence. Scale bars, 5 µm.

to that after KS (**Supplementary Fig. 5b** and **Fig. 3c**). These results demonstrated KS with an N-terminally tagged target and validated KS at the genetic level as well as by complementation. Inactivation of both Rab5a (**Fig. 3**) and PfMon1 (**Supplementary Fig. 4a**) led to a schizont phenotype. This finding may indicate that in *P. falciparum* parasites, similarly to other systems, Mon1 controls Rab5 (ref. 22). The Rab5a phenotype is consistent with data on Rab5 in *Toxoplasma gondii*[23] but is at odds with *P. falciparum* data indicating a role of Rab5a in hemoglobin uptake[21].

SLI and KS enable medium-throughput protein localization and function screens

To test whether our methodology is robust and amenable to medium throughput, we chose *P. falciparum* genes without homology outside Apicomplexans and tagged them with a 2×FKBP-GFP sequence by using SLI (**Fig. 4a**). The selection included eight genes from different chromosomes and ten genes from chromosome 2 as a first step to analyze its genes of unknown function. We obtained the correct integration for all targets, except for three that probably could not be tagged at the C terminus (**Fig. 1b**, **Fig. 4a** and **Supplementary Fig. 1b**). The proteins showed localization in the parasite cytoplasm or the nucleus (**Fig. 4a–c** and **Supplementary Fig. 6**). Candidate 9 was unexpectedly found to be exported, and it represents a new PEXEL-negative exported protein[24] with a cryptic N-terminal signal peptide (**Supplementary Fig. 6**). No GFP fluorescence was detectable for candidate 14, in agreement with its low transcription levels[25]. Because SLI depends on the expression of the additional resistance marker, which is controlled by the promoter of the targeted gene, this candidate illustrates the nearly unrestricted range of transcription levels of the targets for which SLI (using neomycin resistance) is applicable.

We next carried out KS with all the tagged targets (except for the exported candidate). Among the 15 candidates, three could not be mislocalized or exhibited poor mislocalization (**Fig. 4a** and **Supplementary Fig. 6**). For some targets, the number of FKBP domains was doubled to obtain efficient mislocalization (**Fig. 4a**). Growth assays under KS revealed an important function for three candidates, whereas all other tested candidates were not essential for parasite growth (**Fig. 4a–c** and **Supplementary Figs. 3** and **6**).

We conclude that our approach is suitable for medium-throughput screens. As a result of this pilot screen, we localized 14 uncharacterized proteins, three of which are important for parasite proliferation. The growth curves for some of the essential candidates indicated a slow increase in the number of KS parasites 4 d after initiation of rapalog treatment (**Supplementary Fig. 3**).

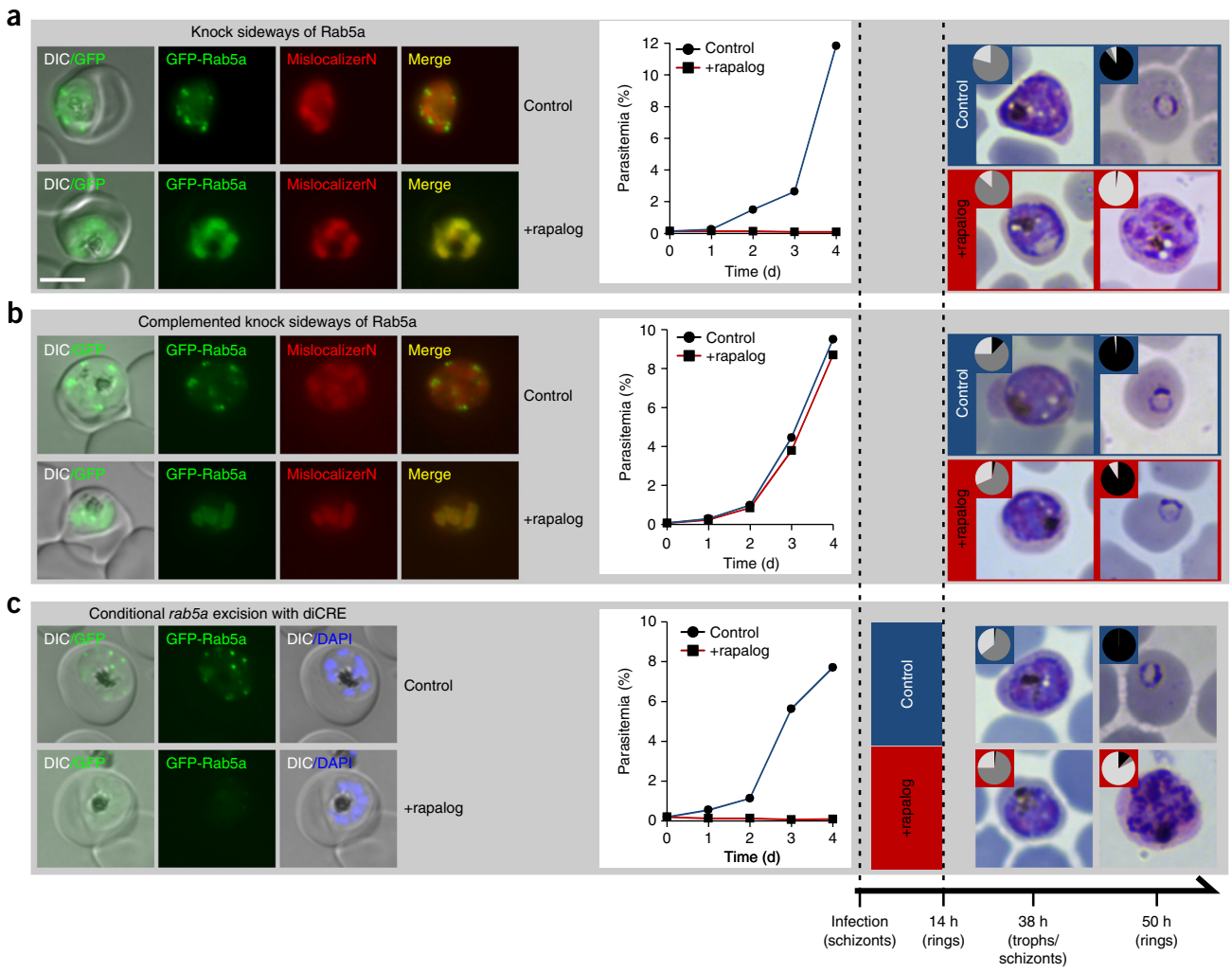

Figure 3 | Functional analysis of N-terminally tagged Rab5a. (**a**–**c**) Cell lines comparing KS (**a**) and KS in the presence of a complementing functional copy of Rab5a (**b**) and after gene excision (**c**). Left, representative fluorescence microscopy images; middle, FC growth curves (one representative of the 3 independent experiments in **Supplementary Fig. 3** is shown). Right, Giemsa smears of synchronous parasites treated with rapalog (red) or control (blue), as indicated (timeline at bottom). Pie charts show quantification of stages (black, rings; dark gray, trophozoites; light gray, schizonts; 38-h control n = 58, 67 and 56 cells for **c**–**e**, respectively; 38-h rapalog n = 59, 60 and 60 for **c**–**e**, respectively; 50-h control n = 53, 57 and 56, for **c**–**e**, respectively; 50-h rapalog n = 54, 55 and 58, for **c**–**e**, respectively; one of 3 independent experiments is shown for each condition). DIC, differential interference contrast; DAPI, parasite nuclei; merge, merged red and green signal; MislocalizerN, nuclear mislocalizer. Scale bars, 5 µm.

An extended growth assay (9 days) with candidate 11 revealed a slowly expanding population of parasites expressing low levels of the mislocalizer (**Supplementary Fig. 7a–c**). Selection of these parasites, despite continued drug pressure to maintain the mislocalizer plasmid, highlights the importance of the target in parasite growth.

We also analyzed the kinetics of mislocalization for four proteins. The time to complete mislocalization was faster (<1 h) in two cytoplasmic proteins compared with two nuclear proteins (**Supplementary Fig. 7d**). These results may indicate that KS performs better for cytoplasmic proteins than for nuclear proteins.

Selectable TGD (SLI-TGD) rapidly identifies genes important for parasite growth

To confirm the KS findings and to provide a complementary approach at the genetic level, we used SLI to select for targeted gene disruptions (TGDs), in an approach that we termed SLI-TGD (**Supplementary Fig. 8**). Using the 18 targets of the localization and KS screen (**Fig. 4a**), we obtained disruptions of all genes that did not show a growth defect after KS (**Fig. 1b** and **Supplementary Fig. 1b**), thus confirming that they were dispensable. In contrast, all our six attempts to disrupt each of the three targets found by KS to be important for parasite growth were unsuccessful (**Fig. 4a**). SLI-TGD also indicated that one of the three targets refractory to mislocalization is important for parasite development. Furthermore, the three genes that could not be C-terminally tagged could not be disrupted with SLI-TGD, thus suggesting an important function for parasite growth. Overall this complementary genetic method correlated with the KS analysis and indicated that 7 out of the 18 targets are important for parasite growth (**Fig. 4a**). Hence, SLI-TGD is a rapid method to disrupt nonessential genes and to determine whether a gene is important for parasite development.

a

No.	Target	SLI (d)	Localization	KS	SLI-TGD
1	PF3D7_0525000	14	Cytosolic/foci	✓	✓
2	PF3D7_0526800	5	Nuclear	✓	✓
3	PF3D7_0720600	x	–	–	x
4	PF3D7_0807600	10	Nuclear	✓*	✓
5	PF3D7_1317400	23	Nuclear	✓*	✓
6	PF3D7_1445700	11	PPM/IMC/cytosolic	x	✓
7	PF3D7_1451200	11	Nuclear	(✓)*	✓
8	PF3D7_1463000	16	Nuclear	✓	✓
9	PF3D7_0202400	14	Exported	ND	✓
10	PF3D7_0205100	x	–	–	x
11	PF3D7_0205600	11	Nuclear	✓ !	x
12	PF3D7_0209700	11	Cytosolic/foci	✓*	✓
13	PF3D7_0210200	9	Nuclear	✓* !	x
14	PF3D7_0211700	23	?	?	✓
15	PF3D7_0210900	21	Nucleus like	✓ !	x
16	PF3D7_0213700	x	–	–	x
17	PF3D7_0213900	11	Cytosolic	x	x
18	PF3D7_0218200	10	Cytosolic	✓	✓

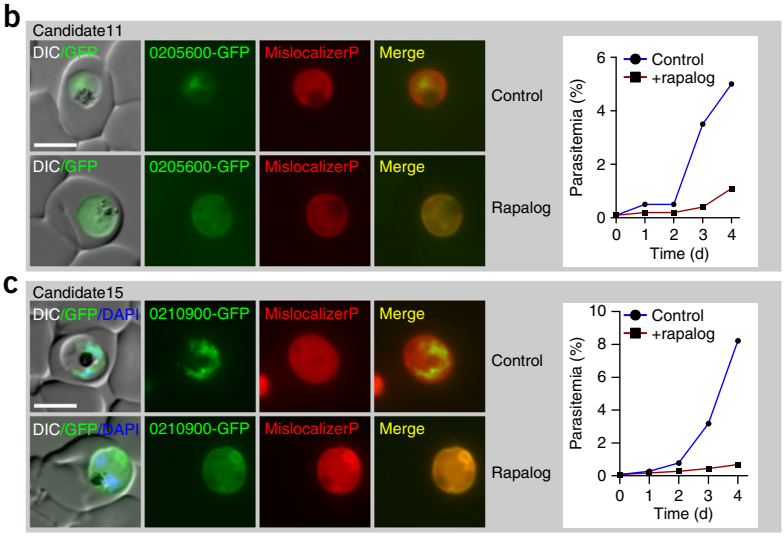

Figure 4 | Localization and functional characterization of unknown *P. falciparum* proteins. (**a**) List of selected genes. The SLI column indicates number of days to integration; check marks in the KS column indicate efficient KS; the check mark in parentheses indicates inefficient mislocalization; exclamation marks indicate targets found to be important for parasite growth; ND, not done; X marks, failure to mislocalize; asterisks, targets with 2×FKBP-GFP-2×FKBP tag; question mark, unclear localization and efficiency of KS, owing to undetectable target. In the SLI-TGD column, checks indicate success (suggesting dispensability), and X marks indicate failure to integrate (suggesting essentiality). (**b**,**c**) Representative live-cell images of two cell lines expressing FKBP-tagged targets found to be important for parasite growth by KS, taken 16 h after induction of KS (rapalog compared with untreated cells (control)). DIC, differential interference contrast; DAPI, parasite nuclei; merge, merged red and green signal; MislocalizerP, plasma-membrane mislocalizer. Scale bars, 5 µm. FC growth curves are shown to the right (one representative of the 3 independent experiments in **Supplementary Fig. 3** is shown).

Analysis of the artemisinin-resistance gene *kelch13*

Finally we targeted Kelch13, the protein implicated in artemisinin resistance[26,27]. Despite the high attention that this protein has received[12], Kelch13 has not been localized or inactivated in previous studies. We performed four attempts each to disrupt the *kelch13* gene by using SLI-TGD or to C-terminally tag it endogenously with a *gfp*-2×*fkbp* sequence by using SLI, all of which failed. Hence, the Kelch13 protein is probably important for parasite survival, and C-terminal tagging impairs its function.

We therefore next modified the N-terminal GFP-FKBP-knockin approach used for Rab5a (**Supplementary Fig. 5a**) to make it selectable through SLI, by adding a skip-peptide-linked second resistance marker to the expression cassette (**Supplementary Fig. 9a**). SLI yielded the correct integration (**Supplementary Figs. 1** and **9b**). The resulting endogenously expressed GFP-2×FKBP-Kelch13 was located in foci in the parasite cytoplasm (**Fig. 5a**). At least one of these foci was usually close to the parasite food vacuole (**Fig. 5a** and **Supplementary Fig. 9c**). In a second SLI-knockin cell line, we inserted a copy of Kelch13 containing a mutation associated with artemisinin resistance (GFP-2×FKBP-Kelch13^{C580Y})[12]. This insertion resulted in parasites that showed increased survival after artemisinin treatment, as compared with the survival of 3D7 or the WT GFP-2×FKBP-K13 knock in (**Fig. 5b**), a result typical for artemisinin resistance[28]. These results confirmed that the inserted copy was active and that the system can also be used to rapidly test resistance alleles.

To assess whether the Kelch13 protein is indeed important for parasite survival, we carried out KS by using a nuclear mislocalizer. After KS, ~90% of the GFP-2×FKBP-Kelch13 population was transferred to the nucleus, but no growth defects were observed (**Supplementary Fig. 9d**). These results indicated that low amounts of the Kelch13 protein are sufficient for parasite survival. We therefore next conditionally eliminated the *kelch13* gene by using diCre. This approach required more than 3 d to deplete the Kelch13 protein, after which growth stopped, and only ring stages remained (**Supplementary Figs. 10a** and **11**). These rings turned into condensed forms over the course of several days (**Supplementary Fig. 10b**).

Although these data showed that Kelch13 is important for parasite survival, the slow disappearance of the protein complicated interpretation of the phenotype. We therefore improved the KS of Kelch13 by using a double 2×FKBP tag, which had been found to improve the mislocalization in our screen (**Fig. 4a**). KS with this cell line (**Supplementary Figs. 1** and **9b**) led to complete mislocalization of Kelch13 and to a rapid-growth phenotype (**Fig. 5c**). When we initiated KS with synchronous ring-stage parasites, we observed an immediate arrest at this stage (**Fig. 5d** and **Supplementary Fig. 11**). Over the next several days, these rings gradually changed into condensed forms (**Fig. 5d**). Hence, the phenotype after diCre-based gene deletion was reproduced and clarified by using KS, which had the benefit of a faster response time. We also created a line for simultaneous diCre-based gene excision and KS, which exhibited a similar phenotype (**Supplementary Figs. 11** and **12**). This combination of both methods may further facilitate protein inactivation for difficult targets.

This study describes what is, to our knowledge, the first localization of the Kelch13 protein and the first direct evidence that this protein is important for parasite survival. Removal of Kelch13 leads to an arrest at the ring stage followed by a slow transition to condensed parasite forms.

DISCUSSION

Currently, endogenous tagging in *P. falciparum* parasites is difficult, and none of the tools for functional analysis described

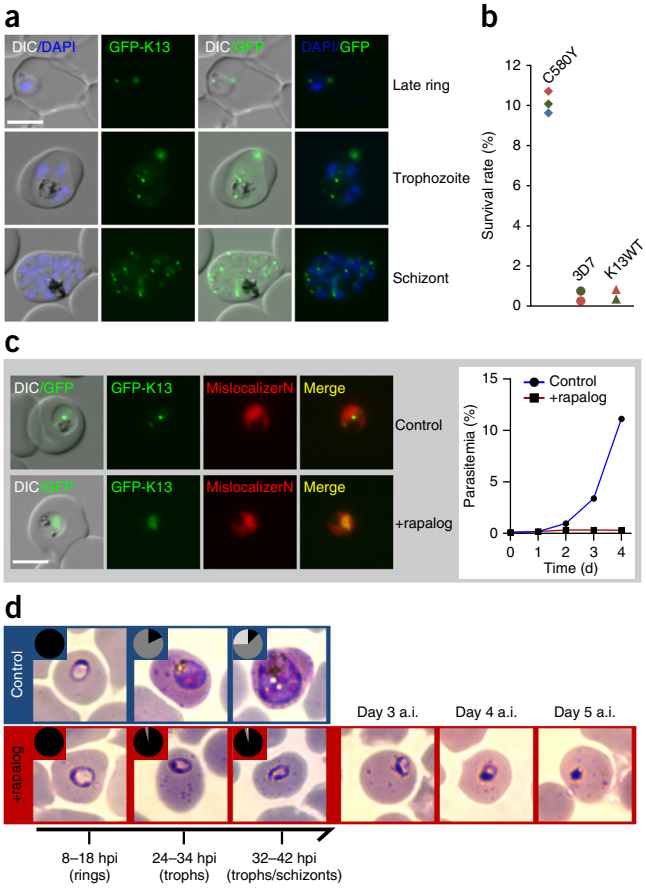

Figure 5 | Analysis of the artemisinin-resistance proteins Kelch13. (**a**) Localization of native N-terminally GFP-tagged Kelch13 (GFP-2×FKBP-Kelch13). (**b**) Graph showing ring-stage survival assays, performed as previously described[28]. Data points show percentage survival of DHA-treated versus untreated parasites for each cell line (n = 3 independent experiments for the GFP-2×FKBP-Kelch13^{C580Y} knockin (C580Y); n = 2 independent experiments for 3D7 and wild-type GFP-2×FKBP-Kelch13 knockin parasites (K13wt)). (**c**) KS with the 2×FKBP-GFP-2×FKBP-Kelch13 parasite line. Left, fluorescence microscopy images of live cells, showing the KS (rapalog) and control. Right, FC growth curve (one representative of 3 independent experiments in **Supplementary Fig. 3** is shown). (**d**) Giemsa-stained smears of synchronous ring stages of 2×FKBP-GFP-2×FKBP-Kelch13 parasites grown with (KS) and without rapalog (control). Timeline and expected stages are indicated below the images. Pie charts show quantification of stages (black, rings; dark gray, trophozoites; light gray, schizonts; n = 119, 105 and 117 control cells and 120, 184 and 118 rapalog-treated cells for the 8–18, 24–34 and 32–42 hours postinvasion (hpi) time points, respectively; one representative of 3 independent experiments is shown). Condensation of arrested rings is shown for days 3, 4 and 5 after induction of KS (a.i.). DIC, differential interference contrast; DAPI, parasite nuclei; merge, merged red and green signal. Scale bars, 5 µm.

to date have proven generally applicable for essential targets (**Supplementary Table 1**). The system presented here should accelerate the study of individual targets and, when combined with appropriate transfection approaches[29], may enable medium- to high-throughput screens. SLI-TGD is expected to replace the traditionally used TGD and may be the method of choice to test the dispensability of genes of interest before more detailed analyses are undertaken, for example, with KS or diCre. The value of localizing all native proteins in an organism has been demonstrated[5], and with SLI this may now be feasible for *P. falciparum*.

Our approaches could also be used to improve existing methods (**Supplementary Table 1**). For instance, SLI can rapidly generate genomic integrations for tagging with FKBP-derived destabilization domains[30]. SLI should hence decrease the often-prohibitive cost arising from the need to apply shield while passively selecting for integration. Insertion of artificial introns with *loxP* sites[31] or addition of glmS ribozymes[32] are further examples that may benefit from SLI.

We also used SLI to rapidly insert mutated alleles, in this case assessing drug resistance. Although this method leaves a larger footprint than those of CRISPR–Cas9 or zinc-finger-generated genome edits (methods that have previously been used to this end in *P. falciparum*[14,27,33]), SLI does not require cloning of parasites and thus permits rapid assessment of many different mutations. SLI also avoids the costs of generating zinc fingers or the need for transfection of two plasmids with CRISPR–Cas9.

KS has proved useful in other systems[6,8,18], and in the present study it worked for most targets (17 out of 20 tested). The double 2×FKBP domain (in pSLI-sandwich) was found to improve the mislocalization and is now the tag of choice. At present, KS cannot be used for secretory proteins; however, the use of hooks to control the release of secretory proteins[34] may present a lead to expand the applicability of KS to such proteins. Together with FKBP-FRB, this independent dimerization system may also enable individual control of two targets in the same cell (further considerations for KS in **Supplementary Note 1**).

Here, we localized and inactivated the artemisinin-resistance protein Kelch13. Our work provides tools and facilitates understanding of resistance to artemisinin and the function of the Kelch13 protein. Overall, we expect this system to be highly useful for the functional study of proteins in *P. falciparum* and other organisms with limited genetic tractability.

METHODS

Methods, including statements of data availability and any associated accession codes and references, are available in the online version of the paper.

Note: Any Supplementary Information and Source Data files are available in the online version of the paper.

ACKNOWLEDGMENTS

We thank F. Kruse (BNITM) for cloning 2×FKBP into pARL-GFP and F. Sanchez-Roman (BNITM) for cloning FKBP into pMSRP6-mDHFR-mCherry. We are grateful to I. Bruchhaus (BNITM) for providing the plasmid pNC. We thank ARIAD Pharmaceuticals for providing plasmids encoding FKBP and FRB. We thank Jacobus Pharmaceuticals for WR99210. The following reagent was obtained through MR4/BEI Resources, NIAID, NIH: DSM1, MRA-1161. S.F., A.B.S. and E.J. gratefully acknowledge funding from the research training group GRK 1459 (German Research Foundation).

AUTHOR CONTRIBUTIONS

J.B., S.F., N.R., A.B.S., P.M.-R., E.J., B.B. and T.S. carried out the experiments. T.S. conceived and coordinated the project. J.B., S.F. and T.S. designed the experiments. T.S. and J.B. arranged the figures, and T.S. drafted the manuscript with input from all authors.

COMPETING FINANCIAL INTERESTS

The authors declare no competing financial interests.

1. World Health Organization. *World Malaria Report 2015* (World Health Organization, 2015).
2. Webster, W.A. & McFadden, G.I. From the genome to the phenome: tools to understand the basic biology of *Plasmodium falciparum*. *J. Eukaryot. Microbiol.* **61**, 655–671 (2014).
3. de Koning-Ward, T.F., Gilson, P.R. & Crabb, B.S. Advances in molecular genetic systems in malaria. *Nat. Rev. Microbiol.* **13**, 373–387 (2015).
4. Woodcroft, B.J., McMillan, P.J., Dekiwadia, C., Tilley, L. & Ralph, S.A. Determination of protein subcellular localization in apicomplexan parasites. *Trends Parasitol.* **28**, 546–554 (2012).
5. Huh, W.K. *et al.* Global analysis of protein localization in budding yeast. *Nature* **425**, 686–691 (2003).
6. Robinson, M.S., Sahlender, D.A. & Foster, S.D. Rapid inactivation of proteins by rapamycin-induced rerouting to mitochondria. *Dev. Cell* **18**, 324–331 (2010).
7. Xu, T., Johnson, C.A., Gestwicki, J.E. & Kumar, A. Conditionally controlling nuclear trafficking in yeast by chemical-induced protein dimerization. *Nat. Protoc.* **5**, 1831–1843 (2010).
8. Haruki, H., Nishikawa, J. & Laemmli, U.K. The anchor-away technique: rapid, conditional establishment of yeast mutant phenotypes. *Mol. Cell* **31**, 925–932 (2008).
9. Jullien, N., Sampieri, F., Enjalbert, A. & Herman, J.P. Regulation of Cre recombinase by ligand-induced complementation of inactive fragments. *Nucleic Acids Res.* **31**, e131 (2003).
10. Andenmatten, N. *et al.* Conditional genome engineering in *Toxoplasma gondii* uncovers alternative invasion mechanisms. *Nat. Methods* **10**, 125–127 (2013).
11. Collins, C.R. *et al.* Robust inducible Cre recombinase activity in the human malaria parasite *Plasmodium falciparum* enables efficient gene deletion within a single asexual erythrocytic growth cycle. *Mol. Microbiol.* **88**, 687–701 (2013).
12. Fairhurst, R.M. Understanding artemisinin-resistant malaria: what a difference a year makes. *Curr. Opin. Infect. Dis.* **28**, 417–425 (2015).
13. Szymczak, A.L. *et al.* Correction of multi-gene deficiency *in vivo* using a single 'self-cleaving' 2A peptide–based retroviral vector. *Nat. Biotechnol.* **22**, 589–594 (2004).
14. Straimer, J. *et al.* Site-specific genome editing in *Plasmodium falciparum* using engineered zinc-finger nucleases. *Nat. Methods* **9**, 993–998 (2012).
15. Wang, P., Wang, Q., Sims, P.F. & Hyde, J.E. Rapid positive selection of stable integrants following transfection of *Plasmodium falciparum*. *Mol. Biochem. Parasitol.* **123**, 1–10 (2002).
16. Geda, P. *et al.* A small molecule-directed approach to control protein localization and function. *Yeast* **25**, 577–594 (2008).
17. Patury, S., Geda, P., Dobry, C.J., Kumar, A. & Gestwicki, J.E. Conditional nuclear import and export of yeast proteins using a chemical inducer of dimerization. *Cell Biochem. Biophys.* **53**, 127–134 (2009).
18. Papanikou, E., Day, K.J., Austin, J. & Glick, B.S. COPI selectively drives maturation of the early Golgi. *eLife* **4**, e13232 (2015).
19. Dvorin, J.D. *et al.* A plant-like kinase in *Plasmodium falciparum* regulates parasite egress from erythrocytes. *Science* **328**, 910–912 (2010).
20. Brancucci, N.M. *et al.* Heterochromatin protein 1 secures survival and transmission of malaria parasites. *Cell Host Microbe* **16**, 165–176 (2014).
21. Elliott, D.A. *et al.* Four distinct pathways of hemoglobin uptake in the malaria parasite *Plasmodium falciparum*. *Proc. Natl. Acad. Sci. USA* **105**, 2463–2468 (2008).
22. Poteryaev, D., Datta, S., Ackema, K., Zerial, M. & Spang, A. Identification of the switch in early-to-late endosome transition. *Cell* **141**, 497–508 (2010).
23. Kremer, K. *et al.* An overexpression screen of *Toxoplasma gondii* Rab-GTPases reveals distinct transport routes to the micronemes. *PLoS Pathog.* **9**, e1003213 (2013).
24. Spielmann, T. & Gilberger, T.W. Protein export in malaria parasites: do multiple export motifs add up to multiple export pathways? *Trends Parasitol.* **26**, 6–10 (2010).
25. Le Roch, K.G. *et al.* Discovery of gene function by expression profiling of the malaria parasite life cycle. *Science* **301**, 1503–1508 (2003).
26. Ariey, F. *et al.* A molecular marker of artemisinin-resistant *Plasmodium falciparum* malaria. *Nature* **505**, 50–55 (2014).
27. Straimer, J. *et al.* Drug resistance. K13-propeller mutations confer artemisinin resistance in *Plasmodium falciparum* clinical isolates. *Science* **347**, 428–431 (2015).
28. Witkowski, B. *et al.* Novel phenotypic assays for the detection of artemisinin-resistant *Plasmodium falciparum* malaria in Cambodia: *in-vitro* and *ex-vivo* drug-response studies. *Lancet Infect. Dis.* **13**, 1043–1049 (2013).
29. Caro, F., Miller, M.G. & DeRisi, J.L. Plate-based transfection and culturing technique for genetic manipulation of *Plasmodium falciparum*. *Malar. J.* **11**, 22 (2012).
30. Armstrong, C.M. & Goldberg, D.E. An FKBP destabilization domain modulates protein levels in *Plasmodium falciparum*. *Nat. Methods* **4**, 1007–1009 (2007).
31. Jones, M.L. *et al.* A versatile strategy for rapid conditional genome engineering using loxP sites in a small synthetic intron in *Plasmodium falciparum*. *Sci. Rep.* **6**, 21800 (2016).
32. Prommana, P. *et al.* Inducible knockdown of *Plasmodium* gene expression using the glmS ribozyme. *PLoS One* **8**, e73783 (2013).
33. Ghorbal, M. *et al.* Genome editing in the human malaria parasite *Plasmodium falciparum* using the CRISPR-Cas9 system. *Nat. Biotechnol.* **32**, 819–821 (2014).
34. Boncompain, G. *et al.* Synchronization of secretory protein traffic in populations of cells. *Nat. Methods* **9**, 493–498 (2012).
35. Varnai, P., Thyagarajan, B., Rohacs, T. & Balla, T. Rapidly inducible changes in phosphatidylinositol 4,5-bisphosphate levels influence multiple regulatory functions of the lipid in intact living cells. *J. Cell Biol.* **175**, 377–382 (2006).

ONLINE METHODS

Step-by-step protocol. A protocol for SLI, KS and FC growth assay is available as **Supplementary Note 2** and in ref. 36.

Plasmid constructs. To generate the SLI knockin constructs, codon-adjusted and linker-flanked 2×FKBP (synthesized by Genscript) was ligated into pARL-GFP[37] to obtain pARL-2×FKBP-GFP. All linkers had previously been used with these domains[35]. The T2A sequence[13,14] was inserted into the fw primer SalI_T2A_Neo_fw used together with Neo_Stop_XhoI_rev (primers in **Supplementary Table 2**) to PCR-amplify the neomycin resistance from plasmid pNC[38] (a kind gift from I. Bruchhaus). This fragment was cloned with SalI/XhoI into pARL-2×FKBP-GFP, at a position after the GFP, thus yielding pSLI-2×FKBP-GFP (maps of key plasmids in **Supplementary Fig. 13**). To double the FKBP tags, 2×FKBP was synthesized with a different codon usage (Genscript), PCR-amplified with primers GFP-2×FKBPfw and GFP-2×FKBPrv, and inserted at the SalI site between GFP and the T2A sequence, thus yielding pSLI-sandwich. Knockin targets were cloned with NotI/AvrII into pSLI-2×FKBP-GFP or pSLI-sandwich by using the C-terminal 533–957 bp, starting with a stop codon and replacing the promoter of the expression cassette in the plasmid. The only exception to this was Mon1, which was cloned in the same way but into pARL-GFP and was integrated conventionally. For SLI-TGD, 231–795 bp shortly downstream of the start ATG of the targets was cloned with NotI/MluI into pARL-2×FKBP-GFP, replacing the promoter and the 2×FKBP tag. This vector was named pSLI-TGD (**Supplementary Fig. 13**).

To obtain the nuclear mislocalizer, linker-flanked FRB* was PCR-amplified from pC_4-RHE (ARIAD) with primer FRB_SpeI_L2_KpnI_rev first and primer XhoI_NLS_MluI_L1_fwd and subsequently with primer L1_NheI_FRB_fwd, thus resulting in 1×NLS-L1-FRB*-L2, which was cloned with XhoI/KpnI into pARL2-MSRP6-mCherry[39]. To obtain three consecutive nuclear localization signals (3×NLS), the fragment was amplified with the primer Mul1_NLS-NLS-L1fw with the same reverse primer and cloned into pARL2mCherry. The *crt* promoter in these constructs was replaced with the *hsp86* promoter by using a PCR fragment generated with primers BglII_Hsp86_promoter_fw and Hsp86_promoter_Xho_rv, to obtain p1×NLS-FRB-mCherry and p3×NLS-FRB-mCherry, respectively (**Supplementary Fig. 13**). For the PPM mislocalizer, the sequence encoding MGCIKSKGKDSAGA[40] was PCR-amplified with primers Lyn-PM-targeting_fw and mCherry_88as, and was cloned with XhoI/NheI into p1×NLS-FRB-mCherry. The promoter was exchanged with the 1,343 bp of the *nmd3* 5′ region (PF3D7_0729300), generated with primers BGlII_NMD3_promoter_fw and NMD3_promoter_Xho_rv, and cloned by using BglII/XhoI to obtain pLyn-FRBmCherry. Alternatively, mislocalizers were expressed in a plasmid providing yDHODH resistance, which was amplified with primers DHODH_backbone_fw and DHODH_backbone_rv, and cloned with BamHI/HindIII into p1×NLS-FRB-mCherry and pLyn-FRBmCherry^{NMD3}, thus yielding p1×NLS-FRB-mCherry-DHODH (used for candidate 12) and pLyn-FRBmCherry-DHODH^{NMD3} (used for candidate 7). An *hsp86*-promoter-driven version of the p1×NLS-FRB-mCherry-DHODH was generated by exchanging the promoter with the *hsp86* 5′ region by using BglII/XhoI, thus yielding pLyn-FRBmCherry^{Hsp86} (used for candidate 15).

For the diCre plasmid, a diCre construct was designed on the basis of the previously published split Cre[9], but FRB* was used instead of FRB, and a skip peptide was used to enable equimolar expression of both fragments from a single expression cassette (**Supplementary Fig. 13**). The corresponding sequence was synthesized (Genscript), PCR-amplified with primers DiCre-XhoI-fwd and DiCre-XmaI-rev, and cloned with XhoI and XmaI (replacing mCherry) into pArl2-MSRP6-mCherry[39], thus yielding the vector pSkipFlox (**Supplementary Fig. 13**).

To obtain the N-terminal Rab5a fusion construct, the linker-flanked 2×FKBP domain was PCR-amplified with primers L-2×fkbp-L-nhei_fwd and L_2×fkbp_L-avrii-rev, and placed downstream of the GPF in pARL-GFP, where a second GFP had previously been cloned upstream (pARL-GFP-GFP) with NheI and AvrII, thus replacing the C-terminal GFP. The *crt* promoter was replaced with the last 700 bp of the *rab5a* genomic coding sequence, excluding the last six bases encoding two cysteines required for prenylation. This region was PCR-amplified with primer rab5a-genomic-700_noti_fwd and four different reverse primers (rab5a-genomic-rev1, rab5a-genomic-rev2, rab5a-genomic-rev3, rab5a-genomic-kpni-rev4), thus yielding a fragment flanked by NotI and KpnI sites and fused to a 2× myc tag, a *loxP* site and the T2A skip peptide. A functional and codon-changed version of *rab5a* with a *loxP* site downstream of the stop codon was synthesized (Genscript), PCR-amplified with primers Rab5a-codon-adjusted-avrii-fwd and Rab5a-codon-adjusted-xhoi-rev, and placed downstream of the 2×FKBP domain with AvrII and XhoI, thus yielding vector p-N-GFP-2×FKBP-loxP (**Supplementary Fig. 13**).

For the complementation of the Rab5A KS, the mCherry sequence (including the stop codon) was removed via KpnI and XmaI from vector p1×NLS-FRB-mCherry. The mCherry sequence (PCR-amplified with primers mcherry-gibson-fwd and mcherry-gibson-rev) and codon-changed *rab5a* (PCR-amplified with primers 2A-rab5A-gibson-fwd and rab5A-gibson-rev) with an upstream T2A skip peptide were then inserted into the vector by Gibson assembly, thus yielding the combined mislocalization and complementation vector p1×NLS-FRB-mCherry-2A-Rab5A.

For the N-terminal SLI of Kelch13, p-N-GFP-2×FKBP-loxP was modified as follows: the *rab5a* genomic sequence was replaced with 544 bp of the genomic *kelch13* sequence (after integration yielded a truncated nonfunctional K13 fragment). This fragment was PCR-amplified with primers Pf06n-term_NotI_fw and Pf06n-term_Pme_rv, and inserted with NotI/PmeI. A functional codon-changed version of *kelch13* was synthesized (Genscript), PCR-amplified with primers Kelch_codon_adjust_fw and Kelch_codon_adjust_rv, and inserted into p-N-GFP-2×FKBP-loxP with AvrII/XhoI, thus resulting in p-N-GFP-2×FKBP-K13-loxP. PCR amplification of the *ydhodh* gene was performed on yeast gDNA with three different fw primers (nTerm-DHODH_fw(1), nTerm-DHODH_fw(2), nTerm-DHODH_fw(3)) and nTerm-DHODH_rv. The fragment was cloned with PmeI/NheI into p-N-GFP-2×FKBP-K13-loxP, thus resulting in the vector pSLI-N-GFP-2×FKBP-K13-loxP. To double the FKBP tags in this vector, 2×FKBP was synthesized with a different codon usage (Genscript), PCR-amplified with primers nT6-DHODH-2×2FKBP_fw and nT6-DHODH-2×2FKBP_rv, and inserted via NheI between GFP and the T2A sequence, thus yielding

doi:10.1038/nmeth.4223

p-N-SLI-sandwich-K13-loxP. To obtain the K13 C580Y mutation, two fragments were amplified by using the codon-changed synthesized version of K13 with primers Kelch_C580Y_fw and Kelch_351-726_rv, as well as Kelch_codon_adjust_fw and Kelch_C580Y_rv. The two fragments were cloned via Gibson assembly into pSLI-N-GFP-2×FKBP-K13-loxP with AvrII/XhoI, thus yielding the vector pSLI-N-GFP-2×FKBP-K13mut-loxP.

To obtain a vector to enable simultaneous KS and diCre excision, 1×NLS-FRB-mCherry was PCR-amplified from p1×NLS-FRB-mCherry in three PCR fragments: primer DiCre_Part2_fw with DiCre_T2A_ca_rv; primer DiCre_T2a_ca_1×NLS_fw with 1×NLS_T2a_DiCre_rv; and primer T2A_DiCre_fw with DiCre_Part1_rv. The three fragments were inserted via Gibson assembly with XhoI/XmaI into pSkipFlox, thus yielding pSkipFlox/1×NLS-FRB-mCherry, which expresses a T2A skip-peptide-flanked 1×NLS-FRB-mCherry between the two diCre fragments.

To obtain the construct for the proof-of-principle FKBP-FRB* mislocalization to the mitochondrion, linker-flanked FKBP was PCR-amplified from pC_4M-F2E (ARIAD) with primers AvrII_linkerL3_FKBP_fwd and FKBP_linkerL4_KpnI_rev, thus replacing mDHFR in pMSRP6-mDHFR-mCherry[39]. Mito-GFP-FRB followed by a skip peptide was PCR-amplified with primers Mito-XhoIfw and FRB*-2A-AvrIIrv, and cloned with XhoI/AvrII, thus replacing MSRP6 and yielding pMito-GFP-FRB-T2A-FKBP-mCherry.

To test SLI by using blasticidin resistance as the SLI selection marker, the genes encoding two exported proteins, the PNEP REX1[41] and the PEXEL protein PFD0095c (PF3D7_0402100), were cloned into REX2mDHFR-int[42], which was used for conventional integration (control), or the vector pSLI-BSD, which was used for SLI. To clone into REX2mDHFR-int, the inserts were PCR-amplified with primers NotI-PFD0095c_F and AvrII-PFD0095c_R or NotI-Rex1_F and AvrII-Rex1_R, and cloned with NotI/AvrII, thus replacing REX2. To obtain pSLI-BSD, T2A-BSD was amplified with primers 2A_fw_AvRII-Nhe and BSD_rv_XhoI, and cloned downstream of the GFP in pARL-2×FKBP-GFP with AvrII/XhoI. The 2×FKBP was then replaced with a synthetic (Genscript) codon-changed mDHFR (PCR-amplified with primers $mDHFR^{recod}$XmaIfw and $mDHFR^{recod}$-KpnIrv), thus inserting an XmaI site before mDHFR to obtain pBSD-SLI. The REX1- and PFD0095c-encoding fragments were cloned into the pBSD-SLI vector in a manner similar to the cloning into REX2mDHFRint but using different reverse primers (XmaI-PFD0095c_R and XmaI-Rex1_R) to allow for use of the NotI and XmaI sites in pSLI-BSD.

Parasite culture, transfection and rapalog experiments. *P. falciparum* parasites (3D7) were cultured at 37 °C in 0+ erythrocytes under standard conditions[43], with RPMI medium supplemented with 0.5% AlbuMAX and microaerophilic conditions. Parasites were transfected with 100 µg of purified plasmid DNA (Qiagen) as previously described[44] or with Amaxa (Lonza) as previously described[45]. Transfectants were selected with 4 nM WR99210 (Jacobus Pharmaceuticals), 2 µg/ml blasticidin S (Invitrogen) or 0.9 µM DSM1 (BEI resources).

SLI and test for correct integration. To select for integrants by using SLI, cultures containing the episomal plasmid selected with WR were adjusted to 2–4% parasitemia, and G418 was added to a final concentration of 400 µg/ml (for SLI with neomycin resistance; 2 µg/mL blasticidin S for blasticidin S resistance; and 1.5 µM DSM1 for yDHODH). WR was not included during this selection phase. These cultures were fed daily until parasites disappeared (up to 10 d) and then were fed every second day. Reappearing parasites were inspected for GFP fluorescence. DNA was prepared with a QIAamp DNA Mini Kit (cat. no. 51304), and PCRs across the integration junctions and testing for leftover unmodified locus (to exclude the presence of wild type or incorrect integrants) were performed (primers in **Supplementary Table 2**). Occasionally, small amounts of wild-type locus were still detected, in which case the culture was placed on WR, thus resulting in a pure integrant culture, as assessed by PCR. For essentiality checks with SLI-TGD, three parallel 5-ml cultures containing the episomal plasmid were placed under G418 selection (400 µg/ml). If no correct integration occurred on two occasions (with a total of six cultures), the target was assumed to be essential.

Knock sideways, diCre induction and flow cytometry growth assays. For the knock sideways and diCre-based gene excision the integrants were transfected with the mislocalizer plasmid or the diCre plasmid and selected with 2 µg/ml blasticidin S. After the transfectants were obtained, if necessary, the blasticidin S concentration was increased stepwise to 9–18 µM, to increase expression levels[46]. For the KS or diCre-based gene excision, the culture was split into two dishes. To one of these dishes, rapalog (AP21967, Clontech) was added to a final concentration of 250 nM (the rapalog was stored at −20 °C as a 500 mM stock in ethanol, and working stocks were kept as 1:20 dilutions in RPMI at 4 °C for a maximum of 3 weeks), and the other dish served as a control. Mislocalization, as compared with the control culture, was verified microscopically after 16 h if not indicated otherwise.

For growth assays, the parasite culture was adjusted to ~0.1% parasitemia and divided into two 2-ml dishes (one with 250 nM rapalog and a control without rapalog). Parasitemia was measured every 24 h for 5 d with an FC assay based on previously described methodology[47]: cultures were resuspended to homogeneity, and 20 µl was placed into a new tube. A mix of 80 µl RPMI, containing Hoechst 33342 (Cheomdex) and dihydroethidium (Cayman) was added to the tube containing the 20-µl cell suspension to obtain final concentrations of 5 µg/ml and 4.5 µg/ml, respectively. Samples were incubated for 20 min at room temperature. Thereafter, 400 µl RPMI containing 0.003% glutaraldehyde was added. Parasitemia was detected as previously described[47], with an LSRII flow cytometer (Becton Dickinson). For every sample, 100,000 events were recorded, and parasitemia was determined with FACSDiva software. Determination of the proportion of ring stages was performed with FlowJo (TreeStar).

Imaging. Microscopy of parasites was performed as previously described[48] with parasites incubated for 10 min with 1 µg/ml DAPI to stain parasite nuclei where appropriate. Images were taken with a Zeiss AxioImager M1 equipped with a Hamamatsu Orca C4742-95 camera. A 100×/1.4–numerical aperture lens or a 63×/1.4–numerical aperture lens was used. Images were processed and overlaid in Corel Photo-Paint. For confocal imaging, parasites were stained with Bodipy-TR-C_5-ceramide (5 µM in RPMI medium) for 30 min at 37 °C as previously described[48], washed in RPMI medium and viewed with a FluoView 1000 confocal

microscope (Olympus) to generate image stacks with a 0.38-µm step size. Three-dimensional reconstructions were generated with Imaris 7.7.2, and maximum-intensity projections were processed in Corel Photo Paint.

All quantifications were performed in ImageJ. To quantify the mislocalization to the mitochondrion in the proof-of-principle experiment, the proportion of background-corrected peak fluorescence at the mitochondrion was compared with the background-corrected fluorescence in the cell cytoplasm. The value obtained for mCherry at mitochondria was adjusted proportionally to the mislocalizer (GFP signal) at mitochondria. The mislocalization of KS targets was quantified with ImageJ by measuring the integrated density of the GFP fluorescence at the original site compared with the integrated density of fluorescence in the nucleus after the baseline fluorescence had been subtracted. For the quantification of the Kelch13 signal after diCre-based gene excision, identical acquisition settings were used for the GFP channel, and the integrated density of fluorescence of individual foci after background fluorescence subtraction was measured. The mCherry fluorescence signal of the mislocalizer after the 9-d FC experiment with candidate 11 was quantified in the same way, but the mean intensity of entire cells was used.

Immunoblots. Western blots were performed essentially as previously described[49]. Parasites were released from iRBCs with 0.015% saponin in 1× PBS, washed in PBS and lysed in 4% SDS, 0.5% Triton X-100 and 0.5× PBS with protease inhibitors (Roche) and frozen at −20 °C. Thawed extracts were centrifuged at 16,000*g*, and Laemmli sample buffer was added to the supernatants. Proteins were separated on polyacrylamide gels and transferred to Amersham Protran membranes (GE Healthcare). Antibody incubations were performed in 5% milk in 1× PBS. Dilutions for primary antibodies were: mouse monoclonal (mixture of clones 7.1 and 13.1) anti-GFP (Roche, 11814460001), 1:1,000; rabbit polyclonal anti-GFP (Thermo, A6455), 1:2,000 and anti-FKBP (Abcam, ab24373), 1:2,500. Secondary antibodies were horseradish peroxidase–conjugated goat anti-mouse (Dianova) diluted 1:3,000 and donkey anti-rabbit (Dianova) diluted 1:2,500. Validation is available on the manufacturers' websites and in **Supplementary Figures 2a** and **9b**. Detection was performed with ECL (Bio-Rad or Thermo), and signals were recorded with a ChemiDoc XRS imaging system (Bio-Rad).

Statistical analysis. All FC growth curves were performed 3 times as independent biological replicates (**Supplementary Fig. 3**). Images of rapalog treated and control parasites are representative of at least 3 independent experiments. Two-sample Wilcoxon rank-sum tests for the comparison of fluorescence intensities after diCre-based excision of the *kelch13* gene were carried out in STATA/SE 10.1 software.

Data availability. The data that support the findings of this study are available from the corresponding author upon request. The key plasmids and their sequences are available from Addgene (no. 73604). Source data files for **Figures 1** and **5** are available online.

36. Birnbaum, J. *et al.* Selection linked integration (SLI) for endogenous gene tagging and knock sideways in *Plasmodium falciparum* parasites. *Protocol Exchange* http://dx.doi.org/10.1038/protex.2017.022 (2017).
37. Crabb, B.S. *et al.* Transfection of the human malaria parasite *Plasmodium falciparum*. *Methods Mol. Biol.* **270**, 263–276 (2004).
38. Meyer, M. *et al.* Overexpression of differentially expressed genes identified in non-pathogenic and pathogenic *Entamoeba histolytica* clones allow identification of new pathogenicity factors involved in amoebic liver abscess formation. *PLoS Pathog.* **12**, e1005853 (2016).
39. Heiber, A. *et al.* Identification of new PNEPs indicates a substantial non-PEXEL exportome and underpins common features in *Plasmodium falciparum* protein export. *PLoS Pathog.* **9**, e1003546 (2013).
40. Tóth, D.J. *et al.* Acute depletion of plasma membrane phosphatidylinositol 4,5-bisphosphate impairs specific steps in endocytosis of the G-protein-coupled receptor. *J. Cell Sci.* **125**, 2185–2197 (2012).
41. Hawthorne, P.L. *et al.* A novel *Plasmodium falciparum* ring stage protein, REX, is located in Maurer's clefts. *Mol. Biochem. Parasitol.* **136**, 181–189 (2004).
42. Mesén-Ramírez, P. *et al.* Stable translocation intermediates jam global protein export in *Plasmodium falciparum* parasites and link the PTEX component EXP2 with translocation activity. *PLoS Pathog.* **12**, e1005618 (2016).
43. Trager, W. & Jensen, J.B. Human malaria parasites in continuous culture. *Science* **193**, 673–675 (1976).
44. Fidock, D.A. & Wellems, T.E. Transformation with human dihydrofolate reductase renders malaria parasites insensitive to WR99210 but does not affect the intrinsic activity of proguanil. *Proc. Natl. Acad. Sci. USA* **94**, 10931–10936 (1997).
45. Moon, R.W. *et al.* Adaptation of the genetically tractable malaria pathogen *Plasmodium knowlesi* to continuous culture in human erythrocytes. *Proc. Natl. Acad. Sci. USA* **110**, 531–536 (2013).
46. Epp, C., Raskolnikov, D. & Deitsch, K.W. A regulatable transgene expression system for cultured *Plasmodium falciparum* parasites. *Malar. J.* **7**, 86 (2008).
47. Malleret, B. *et al.* A rapid and robust tri-color flow cytometry assay for monitoring malaria parasite development. *Sci. Rep.* **1**, 118 (2011).
48. Grüring, C. & Spielmann, T. Imaging of live malaria blood stage parasites. *Methods Enzymol.* **506**, 81–92 (2012).
49. Spielmann, T., Fergusen, D.J. & Beck, H.P. etramps, a new *Plasmodium falciparum* gene family coding for developmentally regulated and highly charged membrane proteins located at the parasite-host cell interface. *Mol. Biol. Cell* **14**, 1529–1544 (2003).

doi:10.1038/nmeth.4223